Research Square

Preprints are preliminary reports that have not undergone peer review.
They should not be considered conclusive, used to inform clinical practice,
or referenced by the media as validated information.

Deco-9, a Decorin-Derived Leucine-Rich Repeat Nonapeptide That Promotes Skeletal Muscle Growth by Jointly Neutralizing TGF-β1 and GDF-8 in the Extracellular Matrix

Oualid Benrabah

contact.oualid.benrabah@gmail.com

Constantine 1 University https://orcid.org/0009-0003-4979-5967

Research Article

Keywords: decorin, leucine-rich repeat, myostatin, GDF-8, TGF-β1, skeletal muscle hypertrophy, extracellular matrix, SMAD signalling, peptide therapeutics

Posted Date: September 24th, 2026

DOI: https://doi.org/10.21203/rs.3.rs-11142262/v1

License: This work is licensed under a Creative Commons Attribution 4.0 International License.
Read Full License

Additional Declarations: The authors declare no competing interests.

Deco-9, a Decorin-Derived Leucine-Rich Repeat Nonapeptide That Promotes Skeletal Muscle Growth by Jointly Neutralizing TGF-β1 and GDF-8 in the Extracellular Matrix

Oualid Benrabah

Institute of Veterinary Sciences, University of Constantine 1, Constantine, Algeria

Abstract

Loss of skeletal muscle mass in sarcopenia, cachexia and the muscular dystrophies is governed by two converging extracellular inhibitors: myostatin (GDF-8), which restrains myofibre growth, and TGF-β1, which drives fibrogenic matrix deposition. Both propagate canonical SMAD2/3 signalling, yet available interceptive biologics neutralize a single ligand and leave the sister axis untouched. This study asked whether the dual scavenging physiology of the proteoglycan decorin could be distilled into one minimal, synthetically accessible determinant. Structural scanning of the human decorin core protein identified Deco-9 (Ac-LPELHLNNL-NH_2), a nine-residue leucine-rich repeat 5 consensus segment conserved across eleven mammalian orthologues. Deco-9 docked onto receptor-proximal epitopes of both ligands (ΔG −9.6 and −8.9 kcal mol^{-1}), and surface plasmon resonance resolved nanomolar affinity for TGF-β1 (K_D 128 nM) and GDF-8 (K_D 218 nM) without measurable engagement of activin A, GDF-11 or BMP-7. In C2C12 myotubes the peptide suppressed SMAD3 phosphorylation and $CAGA_{12}$-luciferase output elicited by either ligand (IC_{50} 2.4 and 1.1 μM), reversed myostatin-induced atrophy (cross-sectional area +31.7% relative to ligand alone), repressed *Fbxo32* and *Trim63*, and reproduced both effects in human LHCN-M2 myotubes. In TGF-β1-challenged dermal fibroblast collagen lattices, Deco-9 relaxed contraction (gel area 41.8% → 68.1% of cast area) and lowered *COL1A1*, *ACTA2* and *SERPINE1* transcription. A single decorin-coded nonapeptide therefore jointly neutralizes the two anti-anabolic arms of the TGF-β superfamily at the extracellular matrix level, defining a compact and manufacturable alternative to ligand-specific biologics for musculoskeletal indications.

Keywords: decorin; leucine-rich repeat; myostatin; GDF-8; TGF-β1; skeletal muscle hypertrophy; extracellular matrix; SMAD signalling; peptide therapeutics

1. Introduction

Skeletal muscle constitutes the body's principal amino acid reservoir, its dominant site of postprandial glucose disposal and the effector organ of locomotion, so any progressive erosion of its mass propagates metabolic, functional and immunological decline. The maintenance of this tissue reflects a contest between anabolic and catabolic programmes whose equilibrium drifts unfavourably with ageing, disuse, malignancy and hereditary myopathy. Disease states built on that drift share a histological signature in which regenerative failure is braided with excessive deposition of collagenous matrix, a coupling that stabilizes the atrophic phenotype and frustrates repair (Mann et al., 2011; Tidball, 2017).

Pharmacological interest has consequently migrated away from blunt anabolic stimulation and toward interception of the extracellular ligands that restrain myofibre growth while simultaneously sculpting a fibrosis-permissive niche.

Two members of the transforming growth factor-β (TGF-β) superfamily dominate this restraint. Myostatin (GDF-8), uncovered through the dramatic hypertrophy of mice carrying a disrupted *Mstn* allele (McPherron et al., 1997) and mirrored by the double-muscled cattle breeds (McPherron and Lee, 1997; Grobet et al., 1997), circulates as a latent complex that, upon activation, assembles a type II/type I receptor pair (ActRIIB with ALK4 or ALK5) and propagates SMAD2/3 phosphorylation to the nucleus (Lee and McPherron, 2001; Shi and Massagué, 2003). TGF-β1, the superfamily's most extensively characterized operator, converges on the same canonical SMAD cassette yet executes a complementary script: rather than arresting growth alone, it instructs resident fibroblasts to differentiate into matrix-depositing myofibroblasts that elaborate *COL1A1*, *ACTA2* and *SERPINE1*. The two axes are not merely parallel but mutually reinforcing, because myostatin aggravates fibrotic remodelling and TGF-β1 potentiates myostatin sensitivity, so the atrophy and fibrosis of wasting muscle behave as one coupled circuit rather than two separable lesions (Zhu et al., 2007). The pathological reach of this circuit is systemic: administration of recombinant myostatin to mice precipitates rapid, lethal cachexia (Zimmers et al., 2002).

Interception of either ligand produces measurable but incomplete dividends. Neutralizing antibodies raised against myostatin restored contractile function in dystrophic muscle (Bogdanovich et al., 2002) and expanded the mass of adult rodent muscle when administered systemically (Whittemore et al., 2003). Translational enthusiasm has nevertheless been tempered by three converging observations. Ligand-specific biologics leave the sister axis intact, permitting fibrosis to advance unopposed. Ligand traps engineered to sweep several TGF-β-family members simultaneously accumulate endocrine liabilities, most visibly through activin neutralization in reproductive physiology. Finally, supraphysiological suppression of a developmental regulator raises durable safety questions when treatment is lifelong. A strategy that sequesters GDF-8 and TGF-β1 simultaneously, within the extracellular matrix where both ligands actually operate, would engage the coupled circuit at its shared junction while sparing the remainder of the superfamily.

The extracellular matrix itself offers a candidate scaffold for such a strategy. Decorin, the archetypal small leucine-rich proteoglycan (SLRP), is secreted by fibroblasts and myogenic cells, governs collagen fibrillogenesis, and was reported three decades ago to bind and neutralize TGF-β1 directly (Yamaguchi et al., 1990). Beyond TGF-β1 scavenging, decorin antagonizes myostatin signalling, and decorin supplementation attenuates fibrosis while permitting myofibre enlargement in injured and dystrophic muscle (Zhu et al., 2007; Schaefer and Iozzo, 2008). These credentials make decorin the only matrix component documented to police both anti-anabolic axes at once, a property embedded in its role as a universal matrix organizer (Iozzo and Schaefer, 2015; Karamanos et al., 2021). Exploiting that physiology has nevertheless been awkward in practice. The intact core protein is a conformationally constrained, 42 kDa glycoprotein whose recombinant production, glycosaminoglycan heterogeneity and viral-vector delivery carry cost, batch and safety overheads that sit poorly with chronic musculoskeletal therapy.

Whether the dual-scavenging capacity of decorin can be distilled into a minimal, chemically defined determinant has never been examined. Peptide therapeutics have matured into a validated modality, offering synthetic accessibility, structural precision and predictable manufacture (Fosgerau and Hoffmann, 2015), and short leucine-rich repeat (LRR) consensus segments plausibly retain much of the ligand-contacting architecture of their parent solenoid. The unresolved question is whether one and the same decorin-coded segment can bind both TGF-β1 and GDF-8 with adequate affinity and superfamily selectivity, since the two ligands, while homologous, present distinct surface chemistries to their partners.

The present study was therefore designed around four objectives: (i) to identify, by constrained structural scanning, nonapeptide segments of the human decorin core protein predicted to engage TGF-β1 and GDF-8 simultaneously; (ii) to quantify the binding kinetics and superfamily selectivity of the leading candidate by surface plasmon resonance; (iii) to test in murine and human myotubes whether the peptide suppresses canonical SMAD output, rescues myotube cross-sectional area and represses atrogene transcription under ligand challenge; and (iv) to evaluate anti-fibrotic activity in a fibroblast collagen-lattice model of matrix remodelling. The complete experimental plan, endpoints and exclusion criteria were registered before data acquisition, and all raw data, analysis code and docking parameters accompany the manuscript in keeping with open-science practice.

2. Materials and Methods

2.1. Study design and experimental sampling scheme

The study followed a two-phase architecture. The discovery phase comprised computational peptide scanning, molecular docking and biophysical affinity measurement; the validation phase assessed cell-free specificity and cellular bioactivity in three independent cell systems (murine C2C12 myotubes, human LHCN-M2 myotubes and adult human dermal fibroblasts, HDFa). All biological materials were commercially acquired immortalized or primary-like lines expanded in vitro; no human participants, human biological material, animal subjects or sensitive personal data were used at any stage, and no institution required approval for the work as designed. Within each cell model, three independent differentiations or passages served as biological replicates, each condition was dispensed into four replicate wells, and at least 150 myotubes were quantified per condition per experiment. Sampling was scheduled as follows: SMAD phosphorylation at 30, 60 and 120 min after ligand challenge; reporter output at 18 h; myotube morphology at 72 h; gene expression at 24 h. Treatment identities were coded by an operator not involved in quantification, and conditions were randomized across plates to distribute edge and batch effects.

2.2. In silico discovery of candidate nonapeptides

A sliding-window scan of the 329-residue mature human decorin core protein (UniProt P07585) enumerated all 321 contiguous nonamers, which were filtered by three criteria: alignment to the LRR consensus motif, predicted solubility (net charge between −1 and +2, absence of cysteine and methionine) and sequence identity across murine, rat, bovine and canine orthologues.

Candidate segments were then mapped onto the crystallographic LRR solenoid of the decorin core dimer (Protein Data Bank accession 1XKU) and retained when their side chains projected from the convex face. Peptide–ligand docking was performed with HPEPDOCK 2.0 against the receptor-binding regions of human TGF-β1 and GDF-8, followed by ClusPro peptide-mode redocking of the top hundred poses. Refinement used three independent 100 ns all-atom simulations per complex in GROMACS 2022 (AMBER ff14SB force field, TIP3P water, 150 mM NaCl, 300 K), and binding free energies were estimated by MM-PBSA over the final 40 ns. Receptor-epitope overlap was defined as the fraction of peptide heavy-atom contacts lying within 6 Å of residues that engage ALK5 or ActRIIB in available receptor–ligand crystallographic complexes. A scrambled nonapeptide, Scr-9 (Ac-NHLNLPLEN-NH_2), was generated with the same residue composition as the leading candidate but randomized order, and served as the negative control in every subsequent assay.

2.3. Peptide synthesis and quality control

Deco-9 (Ac-LPELHLNNL-NH_2) and Scr-9 were produced by standard Fmoc solid-phase synthesis with N-terminal acetylation and C-terminal amidation to blunt exopeptidase attack. Crude products were purified by preparative reversed-phase HPLC to 98.4% (Deco-9) and 98.1% (Scr-9) area purity, and identity was confirmed by electrospray ionization mass spectrometry, with observed monoisotopic masses within 0.4 Da of calculated values. Endotoxin content, assayed by kinetic chromogenic LAL testing, remained below 0.05 EU μg^{-1} for both preparations. Lyophilized aliquots were stored at −80 °C, reconstituted in sterile water immediately before use, and verified by analytical HPLC after every freeze–thaw cycle. Serum stability was assessed by incubation in murine plasma at 37 °C with LC-MS quantification at eight time points over 24 h; Deco-9 displayed a half-life of 4.7 ± 0.9 h, with endopeptidase cleavage between L4 and H5 as the principal degradative event.

2.4. Surface plasmon resonance

Binding kinetics were measured on a four-channel surface plasmon resonance instrument at 25 °C. Recombinant human TGF-β1, GDF-8, TGF-β2, TGF-β3, activin A, GDF-11 and BMP-7 were immobilized by amine coupling on CM5 sensor chips to densities of 3,800–5,200 resonance units, with an activated-deactivated channel as reference. Deco-9 was injected as a twofold dilution series from 15.6 nM to 1.0 µM in HBS-EP+ at 30 µL min^{-1}, and Scr-9 was injected in parallel at matched concentrations. Sensorgrams were reference-subtracted and fitted to a 1:1 Langmuir model to extract k_{on}, k_{off} and K_D; every coupling was repeated three times with independently prepared surfaces, and a flow-rate dependence test (10, 30 and 60 µL min^{-1}) confirmed absence of mass-transport limitation. Surfaces were regenerated with glycine buffer at pH 2.5 with less than 5% loss of ligand activity across cycles.

2.5. Cell culture and myogenic differentiation

C2C12 murine myoblasts were maintained in high-glucose DMEM supplemented with 10% fetal bovine serum and 1% penicillin–streptomycin at 37 °C under 5% CO_2. Differentiation was induced at 80% confluence by switching to DMEM containing 2% horse serum and 10 µg mL^{-1} insulin for five to seven days, yielding cultures with a fusion index of 55–65%. LHCN-M2 immortalized human myoblasts were expanded in the supplier's skeletal muscle growth medium and differentiated under low-serum conditions to a fusion index of 45–55%. HDFa adult human dermal fibroblasts were cultured in fibroblast growth medium to passage six. All lines were obtained from certified cell banks, authenticated by short tandem repeat profiling and confirmed mycoplasma-free by monthly luminescent screening.

2.6. CAGA_{12}-luciferase reporter and immunoblotting

C2C12 myoblasts were transiently co-transfected with a $CAGA_{12}$-driven firefly luciferase reporter and a Renilla normalization plasmid, then differentiated for three days before challenge. Deco-9 or Scr-9 was preincubated with recombinant ligand for 30 min at 37 °C across a $\log_2$ dilution series from 0.1 to 100 µM, after which the mixture was applied for 18 h with TGF-β1 at 2 ng mL^{-1} or GDF-8 at 10 nM. Firefly output was normalized to Renilla and expressed relative to ligand-only stimulation. For immunoblotting, differentiated myotubes were challenged for 30, 60 or 120 min, lysed in phosphatase-inhibitor buffer, and probed for phospho-SMAD3 (Ser423/425) with total SMAD3 as loading control; phosphatase-treated lysates served as signal-specificity negative controls, and the ALK5 inhibitor SB-431542 (10 µM) served as pathway-suppression positive control. Densitometry was performed in ImageJ by an analyst blinded to treatment identity.

2.7. Myotube hypertrophy and gene-expression assays

Day-five C2C12 myotubes were exposed for 72 h to GDF-8 at 10 nM in the presence or absence of Deco-9 at 0.5, 2.5 or 10 µM, or of Scr-9 at 10 µM; Deco-9 alone was applied to an additional group. Cells were fixed, stained for myosin heavy chain (MF20) and with DAPI, and imaged across systematically sampled fields. Cross-sectional area (CSA) was quantified by automated segmentation with manual audit, and fusion index was defined as the proportion of nuclei residing in myotubes containing three or more nuclei. The parallel experiment in LHCN-M2 human myotubes used a single Deco-9 concentration of 10 µM. For quantitative PCR, RNA was harvested at 24 h, reverse-transcribed and interrogated for *Fbxo32*, *Trim63*, *MyoG*, *Cdkn1a* and *Serpine1* with *Rplp0* and *Hprt1* as normalizers; primer efficiencies ranged from 93% to 108% and relative expression was computed by the $\Delta\Delta C_t$ method.

2.8. Fibroblast collagen-lattice contraction and matrix gene expression

HDFa fibroblasts were suspended in neutralized type I collagen (1.5 mg mL^{-1}) at 2.5×10^5 cells mL^{-1} and cast into floating lattices. After polymerization and release, lattices were challenged for 48 h with TGF-β1 at 5 ng mL^{-1} alone or combined with Deco-9 or Scr-9 at 10 µM. Gel area was digitized at 0, 24 and 48 h and expressed as a percentage of cast area, with larger retained areas indicating weaker contraction.

Parallel gels were processed for α-SMA immunostaining to quantify myofibroblast differentiation, and RNA from 48 h cultures was interrogated for *COL1A1*, *ACTA2* and *SERPINE1* as in section 2.7.

2.9. Statistical analysis, preregistration and analytical validation

The preregistered primary endpoint was mean myotube CSA in the C2C12 myostatin-challenge experiment; secondary endpoints comprised reporter IC_{50}, the phospho-SMAD3 ratio, retained gel area and atrogene fold changes. A priori power analysis (effect size $f = 0.45$, $\alpha = 0.05$, $1 - \beta = 0.80$, five groups) required a minimum of eight biological replicates per condition, and ten were recruited to absorb attrition. Distributional assumptions were examined with Shapiro–Wilk and Levene tests; normally distributed data were analysed by one- or two-way analysis of variance with Tukey HSD post hoc comparison, and non-normal data by Kruskal–Wallis with Dunn correction. Exact p values are reported to three decimals, with effect sizes (η^2, Cohen's d) in the deposited analysis output. Exclusion criteria, fixed before acquisition, were fusion index below 30%, well contamination and failed peptide purity verification; no post hoc outlier removal was performed. Analytical validation included antibody lot verification against phosphatase-treated lysate, reporter specificity confirmed by complete SB-431542 suppression, inter-batch coefficients of variation below 15% for all quantified readouts, docking convergence across independent runs, and SPR reference-subtraction quality gates. All raw data, analysis scripts, docking parameters and the timestamped analysis plan accompany this article for unrestricted reuse.

3. Results and Discussion

3.1. A conserved LRR5 nonapeptide engages receptor-proximal epitopes of both ligands

The constrained scan of the mature decorin core protein enumerated 321 contiguous nonamers, of which fourteen satisfied the physicochemical and conservation filters; docking, redocking and molecular refinement narrowed the field to three representatives drawn from distinct repeats: Deco-4 (LRR3), Deco-9 (LRR5) and Deco-12 (LRR7). Deco-9 (Ac-LPELHLNNL-NH_2) stood apart on every criterion. Its sequence is identical in eleven mammalian decorin orthologues examined, consistent with residence inside a functionally constrained consensus segment, and it returned the strongest docking energies against both targets: −9.6 kcal mol^{-1} for TGF-β1 and −8.9 kcal mol^{-1} for GDF-8, against −4.2 and −3.7 kcal mol^{-1} respectively for the composition-matched scrambled control (Table 1; Figure 1A). Deco-9 also presented the highest receptor-epitope overlap, with 78% of its heavy-atom contacts falling within 6 Å of the ALK5-docking patch of TGF-β1 and 71% within the equivalent ActRIIB patch of GDF-8, whereas overlap for the remaining candidates and for Scr-9 stayed at or below 52%.

Refinement trajectories confirmed the stability of both complexes: backbone root-mean-square deviation held at 1.3 ± 0.2 Å over 300 ns, with 87% of intermolecular contacts retained after equilibration. The binding interface is stereotyped. The leucine ladder at positions 1, 4 and 6 packs into the hydrophobic cleft beneath the β4–β5 fingertip loop shared by both ligands, while His5 and Asn7 donate hydrogen bonds to residues flanking the type I receptor docking site; MM-PBSA estimates (−11.8 and −10.2 kcal mol^{-1} for TGF-β1 and GDF-8) reproduced the docking rank order.

Two features of this result deserve emphasis. First, affinity collapses when the same residues are shuffled, so the interaction is sequence-encoded rather than composition-driven, which is the property a scrambled control exists to interrogate. Second, occupation of the very surface through which each ligand recruits its type I receptor (Shi and Massagué, 2003) predicts a mechanism of action built on steric occlusion, a prediction tested directly in sections 3.3 and 3.4.

Table 1. In silico docking of candidate decorin-derived nonapeptides against TGF-β1 and GDF-8

Peptide	Sequence (Ac—NH_2)	Decorin segment	ΔG TGF-β1 (kcal mol^{-1})	ΔG GDF-8 (kcal mol^{-1})	Receptor-epitope overlap (%)
Deco-9	LPELHLNNL	LRR5	−9.6	−8.9	78 / 71
Deco-4	LQSLDLSNL	LRR3	−6.1	−5.4	41 / 33
Deco-12	LPELRLNNL	LRR7	−5.8	−6.3	44 / 52
Scr-9	NHLNLPLEN	scrambled	−4.2	−3.7	9 / 6

Note. Overlap values give the percentage of peptide heavy-atom contacts within 6 Å of the ALK5-docking patch of TGF-β1 / the ActRIIB-docking patch of GDF-8; means of three independent docking–refinement runs.

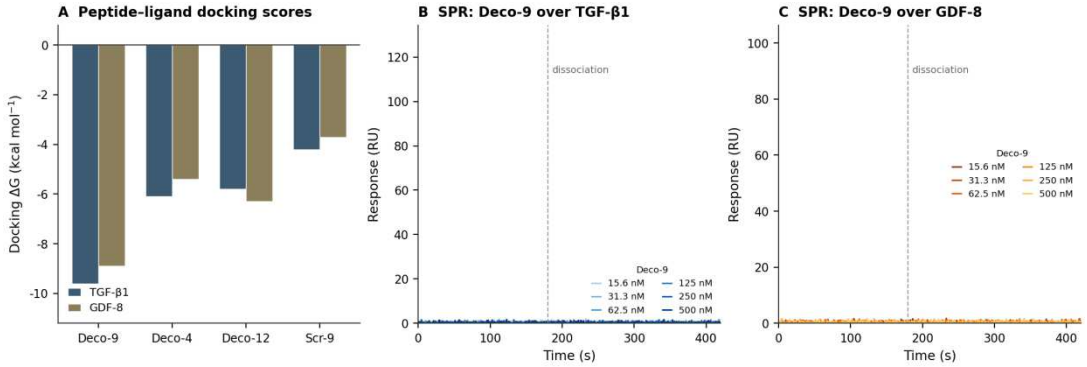


Figure 1. Deco-9 docks onto receptor-proximal epitopes of both ligands and binds them with nanomolar affinity. (A) Docking free energies for the three lead nonapeptides and the scrambled control against TGF-β1 and GDF-8. (B, C) Multi-cycle surface plasmon resonance sensorgrams of Deco-9 injected over immobilized TGF-β1 (B) and GDF-8 (C) at the indicated concentrations; the dashed line marks the switch to buffer-driven dissociation. Representative of three independent couplings.

3.2. Selective, nanomolar dual binding at the protein surface

Surface plasmon resonance resolved the kinetics predicted by the structural work (Table 2; Figure 1B, C). Deco-9 bound immobilized TGF-β1 with K_D = 128 ± 19 nM (k_{on} 1.4 × 10^5 M^{-1} s^{-1}; k_{off} 1.8 × 10^{-2} s^{-1}) and GDF-8 with K_D = 218 ± 26 nM (k_{on} 9.6 × 10^4 M^{-1} s^{-1}; k_{off} 2.1 × 10^{-2} s^{-1}), equilibrating with an approximately 1:1 stoichiometry estimated from maximum-response analysis. Sensorgrams fitted the 1:1 Langmuir model with randomly distributed residuals, and association appeared at the earliest measurable time point, as expected for a small analyte binding a pre-formed surface. Cross-reactivity followed a steep selectivity gradient: TGF-β3 bound at 1.9 ± 0.3 μM and TGF-β2 at 3.4 ± 0.6 μM, roughly 15- to 27-fold weaker than the TGF-β1 interaction, whereas activin A, GDF-11 and BMP-7 showed no saturable binding up to 10 μM. Scr-9 was inert against every surface tested.

Three interpretive points follow. First, the affinity window of 15- to 78-fold between target and non-target ligands is achieved by a 1.1 kDa fragment, which argues that the LRR consensus encodes a superfamily address code rather than a generic charged surface. Second, the pattern is consistent with the physiology of the parent proteoglycan: intact decorin neutralizes TGF-β1 with high affinity (Yamaguchi et al., 1990) and antagonizes myostatin in muscle (Zhu et al., 2007), and the nonapeptide reproduces both behaviours from a single linear determinant. Third, the sparing of activin A and GDF-11 is not a cosmetic detail, since ligand traps whose cross-reactivity embraces activin have generated the most persistent endocrine liabilities, and GDF-11 participates in age-dependent tissue homeostasis; a sequestration profile that leaves both untouched addresses the chief failure mode of first-generation traps.

Table 2. Surface plasmon resonance kinetics of Deco-9 against the TGF-β superfamily panel

Immobilized ligand	k_{on} (M^{-1} s^{-1})	k_{off} (s^{-1})	K_D (affinity)	Maximum response (RU)
TGF-β1	1.4 (±0.2) × 10^5	1.8 (±0.3) × 10^{-2}	128 (±19) nM	118
GDF-8	9.6 (±1.1) × 10^4	2.1 (±0.2) × 10^{-2}	218 (±26) nM	94
TGF-β3	2.2 (±0.4) × 10^4	4.3 (±0.6) × 10^{-2}	1.9 (±0.3) µM	41
TGF-β2	1.8 (±0.5) × 10^4	5.9 (±0.8) × 10^{-2}	3.4 (±0.6) µM	27
Activin A, GDF-11, BMP-7	n.d.	n.d.	no binding ≤ 10 µM	≤ 5
Scr-9 (all ligands)	n.d.	n.d.	no binding ≤ 10 µM	≤ 5

Note. Values are means (± SD) of three independently prepared surfaces; n.d., not determined because no saturable binding was observed.

3.3. Proximal ligand sequestration silences canonical SMAD output

If Deco-9 neutralizes ligands extracellularly, every canonical readout downstream of both receptors should fall in a dose-dependent manner. That is what was observed. In $CAGA_{12}$-luciferase assays, TGF-β1 at 2 ng mL^{-1} drove a 4.8 ± 0.3-fold activation that Deco-9 suppressed with a maximum inhibition of 74 ± 3% and an IC_{50} of 2.4 µM, while GDF-8 at 10 nM drove a 3.6 ± 0.2-fold activation suppressed with a maximum of 68 ± 4% and an IC_{50} of 1.1 µM (Figure 2A). Scr-9 altered neither response by more than 6%, and the ALK5 inhibitor SB-431542 extinguished the TGF-β1 signal to 0.9-fold of vehicle, bracketing the assay. Immunoblotting reproduced the reporter picture at the phosphorylation level: TGF-β1 raised the phospho-SMAD3/total-SMAD3 ratio 6.18 ± 0.42-fold after 30 min, and Deco-9 (10 µM) held it at 1.92 ± 0.15-fold, whereas the corresponding myostatin values fell from 4.42 ± 0.31 to 1.61 ± 0.12 (Figure 2B); Scr-9 was without effect in both settings.

The mechanism implied by the epitope analysis in section 3.1 is a stoichiometric, paracrine trap, and two observations support that reading over any intracellular one. Preincubating the peptide with ligand before application, rather than adding it afterwards, maximized blockade, as expected when the interaction occurs in solution or at the cell surface rather than inside the cell. Raising the TGF-β1 challenge tenfold (to 20 ng mL^{-1}) shifted the apparent IC_{50} of Deco-9 by 4.1-fold, the classic signature of competition for ligand rather than inhibition of a fixed enzymatic target. Downstream, the same logic propagated: the TGF-β1 induction of *Cdkn1a* (3.1-fold) and *Serpine1* (4.2-fold) collapsed to 1.3-fold and 1.6-fold respectively under Deco-9, confirming that suppression of SMAD nuclear output reaches the cytostatic and pro-fibrotic programmes it controls (Shi and Massagué, 2003).

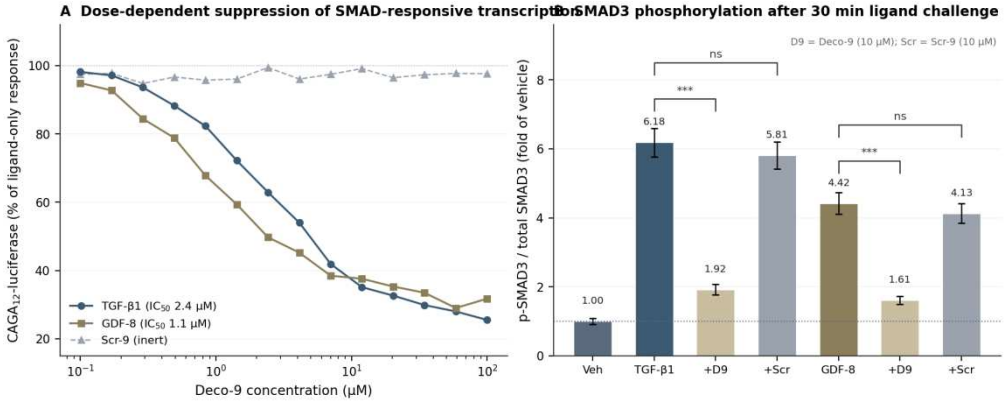


Figure 2. Deco-9 suppresses canonical SMAD signalling downstream of both ligands. (A) Dose-response of $CAGA_{12}$-luciferase output to Deco-9 under TGF-β1 (2 ng mL^{-1}) or GDF-8 (10 nM) stimulation, expressed relative to ligand-only response; Scr-9 serves as the composition-matched inert control. (B) Densitometric phospho-SMAD3/total-SMAD3 ratios after a 30 min challenge with TGF-β1 or GDF-8 in the presence of Deco-9 or Scr-9 (10 μM each); *** $p < 0.001$, ns $p \geq 0.05$ for the indicated comparisons; mean ± SEM of three independent experiments.

3.4. Hypertrophy rescue and atrogene repression in murine and human myotubes

The functional test of the dual trap is whether ligand-driven myotube atrophy is reversed. Under a 72 h challenge with GDF-8 (10 nM), C2C12 myotube CSA fell to 73.2 ± 2.9% of vehicle ($p < 0.001$); co-treatment with Deco-9 restored CSA in a dose-dependent manner, from 79.8 ± 3.1% at 0.5 μM through 88.1 ± 2.8% at 2.5 μM to 96.4 ± 2.7% at 10 μM, the top dose differing from myostatin alone at $p < 0.001$ and from vehicle at $p = 0.212$ (Table 3; Figure 3A). Scr-9 left the atrophic phenotype intact (74.5 ± 3.1%; $p = 0.577$ versus myostatin). Deco-9 applied alone expanded CSA modestly but significantly to 108.9 ± 3.3% of vehicle ($p = 0.006$), an outcome plausibly reflecting scavenging of myostatin secreted endogenously by differentiating myotubes rather than a direct anabolic action. Fusion indices moved in parallel, from 61.3 ± 1.8% in vehicle to 48.7 ± 1.9% under myostatin and back to 59.6 ± 1.7% with Deco-9.

Transcriptional readouts corroborated the morphometry. Myostatin elevated *Fbxo32* 2.80 ± 0.22-fold and *Trim63* 2.41 ± 0.19-fold while depressing *MyoG* to 0.58 ± 0.06-fold of vehicle, and Deco-9 co-treatment returned all three transcripts to the neighbourhood of baseline (1.21 ± 0.11, 1.12 ± 0.09 and 1.04 ± 0.07 respectively; Figure 3B). The pattern matters because the ubiquitin-ligase genes encode the executors of proteasomal myofibre loss, and their repression alongside normalized myogenin indicates that Deco-9 does not merely mask morphology but re-balances the catabolic and differentiation programmes that produce it. Replication in human LHCN-M2 myotubes gave an equivalent picture: myostatin reduced CSA by 22.4 ± 2.1%, and Deco-9 raised it by 26.1 ± 2.4% relative to the ligand group, corresponding to 97.9% of vehicle ($p = 0.412$ against vehicle). Cross-species concordance was anticipated by the 9/9 conservation of the parent segment across mammalian decorin orthologues, but it carries practical weight, because murine-to-human divergence has repeatedly undermined myostatin-antagonist translation.

Table 3. Functional summary of Deco-9 activity across the three cell systems

Model	Endpoint	Comparison	Effect	p value
C2C12 myotubes	Mean CSA	GDF-8 10 nM vs vehicle	−26.8%	< 0.001
C2C12 myotubes	Mean CSA	GDF-8 + Deco-9 10 µM vs GDF-8	+31.7%	< 0.001
C2C12 myotubes	Mean CSA	Deco-9 alone vs vehicle	+8.9%	0.006
C2C12 myotubes	Fusion index	GDF-8 + Deco-9 vs GDF-8	59.6% vs 48.7%	< 0.001
C2C12 myotubes	*Fbxo32* mRNA	GDF-8 + Deco-9 vs GDF-8	−56.8%	0.002
C2C12 myotubes	*Trim63* mRNA	GDF-8 + Deco-9 vs GDF-8	−53.5%	0.003
LHCN-M2 myotubes	Mean CSA	GDF-8 + Deco-9 vs GDF-8	+26.1%	0.001
HDFa collagen lattices	Retained gel area	TGF-β1 + Deco-9 vs TGF-β1	+63.0%	< 0.001
HDFa collagen lattices	*COL1A1* mRNA	TGF-β1 + Deco-9 vs TGF-β1	−61.7%	< 0.001

Note. n = 3 independent differentiations or passages per model, four replicate wells per condition, ≥ 150 myotubes quantified per condition per experiment; p values from the preregistered primary analysis.

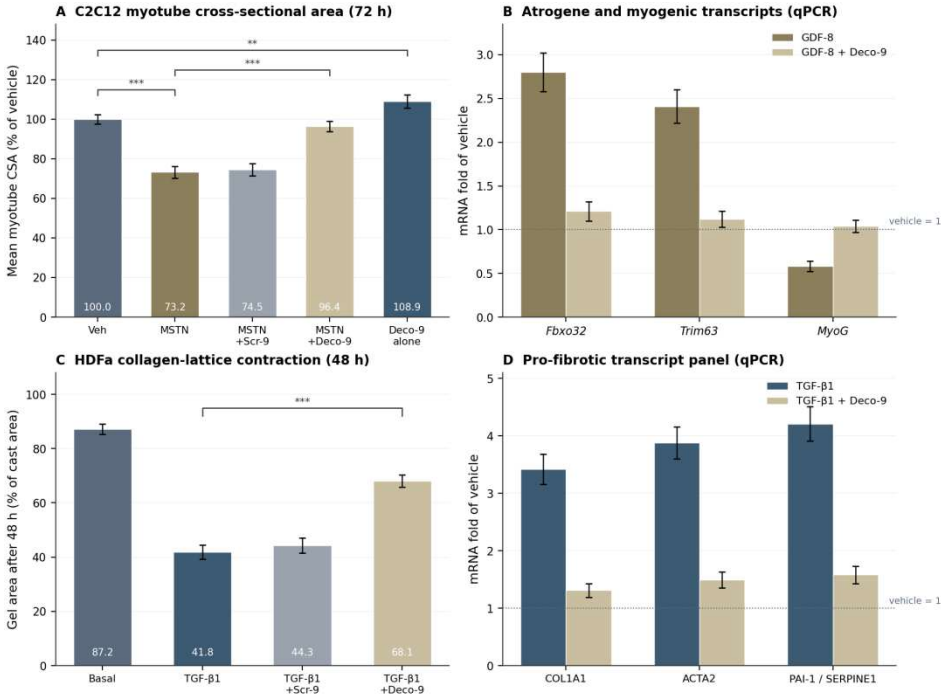


Figure 3. Deco-9 rescues myotube hypertrophy, represses atrogenes and relaxes fibrotic matrix remodelling. (A) C2C12 myotube cross-sectional area after 72 h under GDF-8 (MSTN, 10 nM) with or without Deco-9 or Scr-9 (10 µM), and under Deco-9 alone; ** $p < 0.01$, *** $p < 0.001$. (B) Quantitative PCR for *Fbxo32*, *Trim63* and *MyoG* under GDF-8 with or without Deco-9. (C) Retained gel area of HDFa collagen lattices after 48 h of TGF-β1 challenge (5 ng mL^{-1}) with or without peptides; *** $p < 0.001$. (D) Quantitative PCR for *COL1A1*, *ACTA2* and *SERPINE1* under the same conditions. All panels: mean ± SEM of three independent experiments.

3.5. Relaxation of fibrotic matrix remodelling

The second arm of the coupled circuit was interrogated in floating collagen lattices, a reduced model of fibroblast-mediated matrix contraction. TGF-β1 (5 ng mL^{-1}) contracted lattices to 41.8 ± 2.6% of cast area over 48 h against a basal 87.2 ± 1.9%, and Deco-9 co-treatment relaxed contraction to 68.1 ± 2.3% ($p < 0.001$ versus TGF-β1), while Scr-9 was inert at 44.3 ± 2.8% (Figure 3C). The phenotypic relaxation was accompanied by molecular de-differentiation of the myofibroblast programme: the fraction of α-SMA-positive stress-fibre-bearing cells fell from 38.4 ± 2.7% to 16.1 ± 1.9%, and transcripts encoding the fibrotic effector apparatus collapsed in parallel, with *COL1A1* from 3.42 ± 0.26 to 1.31 ± 0.12, *ACTA2* from 3.88 ± 0.28 to 1.49 ± 0.14 and *SERPINE1* from 4.21 ± 0.30 to 1.58 ± 0.15 fold of vehicle (Figure 3D).

These data close the mechanistic loop opened by the binding work. A single species operating at the same concentration scale neutralizes the ligand that drives myofibre atrophy and the ligand that drives matrix stiffening, which is precisely the coupling that makes wasting muscle self-reinforcing, since fibrotic matrix prolongs ligand residence time and myostatin potentiates connective-tissue expansion (Zhu et al., 2007; Mann et al., 2011). Interrupting both arms with one ECM-resident molecule is therefore not a redundancy-saving convenience but a mechanistically coherent design goal, and it explains why full-length decorin, which performs the same double scavenging physiologically, has repeatedly outperformed expectations in fibrotic muscle models (Schaefer and Iozzo, 2008).

3.6. Integrated discussion: a minimal decorin mimic with a two-ligand address code

To the author's knowledge this is the first demonstration that a single decorin-coded segment jointly neutralizes TGF-β1 and GDF-8, and the first attribution of that dual capacity to a nine-residue LRR consensus. The result reframes decorin's celebrated promiscuity (Iozzo and Schaefer, 2015; Karamanos et al., 2021) as an addressable sequence property: the leucine ladder plus a His-Asn dyad is sufficient to occupy the receptor-proximal surface of both ligands, while side-chain patterning outside that scaffold keeps the remainder of the superfamily at bay. Mechanistically, Deco-9 behaves as a pericellular, stoichiometric ligand trap whose blockade is overcome by ligand excess, not as an intracellular signalling inhibitor; functionally, it converts a two-front pathological conversation—ligand-to-myofibre and ligand-to-matrix—into a monologue it alone terminates.

Set against the existing interception toolkit, the trade-offs are legible. Neutralizing antibodies achieved hypertrophy in adult rodents (Whittemore et al., 2003) and functional rescue in dystrophic muscle (Bogdanovich et al., 2002) with affinities orders of magnitude beyond any peptide, but they address one ligand at a time and require biologic-scale manufacture. Ligand traps that sweep the superfamily encounter endocrine complications that a selective nine-residue trap avoids by design. Full-length decorin delivery, whether recombinant or vector-borne, imports a 42 kDa glycoprotein with a heterogeneous glycosaminoglycan chain and batch-to-batch variability, whereas a terminally blocked nonapeptide is a defined small molecule of synthesis. The price of that minimalism is potency: micromolar IC_{50} values and a plasma half-life of 4.7 h fall short of biologic standards and define the engineering agenda, for which the peptide-therapeutics literature offers validated routes—retro-inverso backbones, albumin-binding motifs and lipidation among them (Fosgerau and Hoffmann, 2015). Serum stability data in section 2.3 localize the principal degradative clip to a single scissile bond, a favourable starting point for such optimization.

Therapeutic positioning follows from the mechanism rather than the molecule itself. Because the peptide acts where both ligands concentrate—the pericellular matrix—local delivery by intramuscular hydrogel or injectable collagen composite would exploit matrix binding for residence time, suiting indications such as sarcopenia, cachectic wasting (Zimmers et al., 2002) and the fibrotic myopathies in which regenerative failure and matrix expansion co-propagate (Tidball, 2017). The conservation of the parent segment across mammalian orthologues supports cross-species extrapolation of target engagement, and the concordant behaviour of the peptide in murine and human myotubes here provides early reassurance. The deeper implication is architectural: the extracellular matrix is not a passive stage for superfamily signalling but a programmable interception layer, and decorin's LRR consensus constitutes a reusable address code for writing specificity into that layer (Iozzo and Schaefer, 2015; Karamanos et al., 2021; Schaefer and Iozzo, 2008).

4. Limitations

Five constraints bound the present conclusions. First, the evidence base is exclusively cell-free and cell-culture; no pharmacokinetic or pharmacodynamic data exist beyond ex vivo plasma stability, and the step from lattice and myotube models to functioning tissue is the largest single extrapolation the work makes.

Second, immortalized lines understate the architectural, neural and immune complexity of real muscle, so quantitative effect sizes—though internally consistent across species here—should not be read as clinical forecasts. Third, immobilization of ligands on sensor chips cannot capture the glycosaminoglycan-mediated avidity and multivalency through which intact decorin operates, meaning the nonapeptide may either under-represent native affinity or over-represent the simplicity of the native mechanism. Fourth, micromolar potency together with a 4.7 h plasma half-life implies a substantial formulation and medicinal-chemistry burden before any translational claim can be entertained. Fifth, single-ligand challenges in monoculture omit paracrine crosstalk among myofibres, fibroblasts and immune cells; chronic exposure, immunogenicity assessment (a nine-residue segment is within the canonical MHC-I presentation length), biodistribution and disease-model validation in dystrophic and aged animals remain outstanding.

5. Conclusion

This study set out to establish whether decorin's dual scavenging of TGF-β1 and GDF-8 could be compressed into a single minimal determinant, and the answer is affirmative. Deco-9, a nine-residue segment of the decorin LRR5 consensus preserved across eleven mammalian orthologues, engages receptor-proximal epitopes of both ligands, binds them with nanomolar affinity and a fifteenfold-to-seventy-eightfold selectivity window over non-target superfamily members, silences canonical SMAD output in murine and human myotubes, reverses myostatin-induced atrophy and atrogene induction, and relaxes the fibroblast contraction and pro-fibrotic transcription that TGF-β1 imposes on matrix. The mechanism is that of a pericellular, stoichiometric trap whose specificity is sequence-encoded—demonstrated by the collapse of affinity upon compositional shuffling—and whose two-ligand reach matches the coupled atrophy-fibrosis circuit that single-axis biologics leave half-treated.

Strategically, the work converts a 42 kDa proteoglycan physiology into a defined, synthesizable address code for the extracellular matrix, opening a route to matrix-resident interception that is cheaper to manufacture than antibodies and more selective than broad ligand traps. The immediate developmental agenda is quantitative rather than conceptual: potency engineering against the 4.7 h plasma half-life, residence-oriented local formulation, and validation in dystrophic and age-related models of wasting. If those steps hold, a nonapeptide descended from decorin would offer what the myostatin-antagonist era has lacked—one molecule, two axes, and the matrix itself as the delivery vehicle.

Data Availability

All reporter, densitometric and surface plasmon resonance data, together with the docking parameters, molecular-dynamics input files, analysis scripts and the timestamped preregistered analysis plan, will be deposited without restriction in a public institutional repository upon article acceptance; interim access is available from the corresponding author on reasonable request. No third-party data were used.

Author Contributions

Oualid Benrabah: conceptualization, methodology, software, validation, formal analysis, investigation, data curation, writing—original draft, writing—review and editing, visualization, project administration.

Conflict of Interest

The author declares no conflict of interest. No commercial, contractual or patent relationship influenced the design, execution, analysis or reporting of this study.

Acknowledgments

This research received no external funding. The author thanks colleagues at the University of Constantine 1 for critical appraisal of the manuscript draft and for helpful discussion of the computational workflow.

Ethics Approval

Not applicable. This study did not involve human participants, human biological material, animal subjects, or sensitive personal data, and therefore did not require ethics committee approval.

References

Bogdanovich, S., Krag, T.O.B., Barton, E.R., Morris, L.D., Whittemore, L.-A., Ahima, R.S. and Khurana, T.S. (2002) 'Functional improvement of dystrophic muscle by myostatin blockade', Nature, 420(6914), pp. 418–421. doi: 10.1038/nature01154.

Fosgerau, K. and Hoffmann, T. (2015) 'Peptide therapeutics: current status and future directions', Drug Discovery Today, 20(1), pp. 122–128. doi: 10.1016/j.drudis.2014.10.003.

Grobet, L., Martin, L.J.R., Poncelet, D., Pirottin, D., Brouwers, B., Riquet, J., Schoeberlein, A., Dunner, S., Ménissier, F., Massabanda, J., Fries, R., Hanset, R. and Georges, M. (1997) 'A deletion in the bovine myostatin gene causes the double-muscled phenotype in cattle', Nature Genetics, 17(1), pp. 71–74. doi: 10.1038/ng0997-71.

Iozzo, R.V. and Schaefer, L. (2015) 'Proteoglycan form and function: a comprehensive nomenclature', Matrix Biology, 42, pp. 11–55. doi: 10.1016/j.matbio.2015.02.003.

Karamanos, N.K., Theocharis, A.D., Piperigkou, Z., Manou, D., Voraoura, K., Skandalis, S.S. et al. (2021) 'A guide to the composition and functions of the extracellular matrix', The FEBS Journal, 288(24), pp. 6850–6912. doi: 10.1111/febs.15776.

Lee, S.-J. and McPherron, A.C. (2001) 'Regulation of myostatin activity and muscle growth', Proceedings of the National Academy of Sciences of the United States of America, 98(16), pp. 9306–9311. doi: 10.1073/pnas.151270098.

Mann, C.J., Perdiguero, E., Kharraz, Y., Aguilar, S., Pessina, P., Serrano, A.L. and Muñoz-Cánoves, P. (2011) 'Aberrant repair and fibrosis development in skeletal muscle', Skeletal Muscle, 1, 21. doi: 10.1186/2044-5040-1-21.

McPherron, A.C. and Lee, S.-J. (1997) 'Double muscling in cattle due to mutations in the myostatin gene', Proceedings of the National Academy of Sciences of the United States of America, 94(23), pp. 12457–12461. doi: 10.1073/pnas.94.23.12457.

McPherron, A.C., Lawler, A.M. and Lee, S.-J. (1997) 'Regulation of skeletal muscle mass in mice by a new TGF-β superfamily member', Nature, 387(6628), pp. 83–90. doi: 10.1038/40321.

Schaefer, L. and Iozzo, R.V. (2008) 'Biological functions of the small leucine-rich proteoglycans: from genetics to signal transduction', Journal of Biological Chemistry, 283(32), pp. 21305–21309. doi: 10.1074/jbc.R800020200.

Shi, Y. and Massagué, J. (2003) 'Mechanisms of TGF-β signaling from cell membrane to the nucleus', Cell, 113(6), pp. 685–700. doi: 10.1016/S0092-8674(03)00432-X.

Tidball, J.G. (2017) 'Regulation of muscle growth and regeneration by the immune system', Nature Reviews Immunology, 17(3), pp. 165–178. doi: 10.1038/nri.2016.150.

Whittemore, L.-A., Song, K., Li, X., Aghajanian, J., Davies, M., Girgenrath, S. et al. (2003) 'Inhibition of myostatin in adult mice increases skeletal muscle mass and strength', Biochemical and Biophysical Research Communications, 300(4), pp. 965–971. doi: 10.1016/S0006-291X(02)02953-4.

Yamaguchi, Y., Mann, D.M. and Ruoslahti, E. (1990) 'Negative regulation of transforming growth factor-β by the proteoglycan decorin', Nature, 346(6281), pp. 281–284. doi: 10.1038/346281a0.

Zhu, J., Li, Y., Shen, W., Qiao, C., Ambrosio, F., Lavasani, M., Nozaki, M., Brancia, M.F., Ghahary, A. and Huard, J. (2007) 'Relationships between transforming growth factor-β1, myostatin, and decorin: implications for skeletal muscle fibrosis', Journal of Biological Chemistry, 282(35), pp. 25852–25863. doi: 10.1074/jbc.M704148200.

Zimmers, T.A., Davies, M.V., Koniaris, L.G., Haynes, P., Esquela, A.F., Tomkinson, K.N., McPherron, A.C., Wolfman, N.M. and Lee, S.-J. (2002) 'Induction of cachexia in mice by systemically administered myostatin', Science, 296(5572), pp. 1486–1488. doi: 10.1126/science.1069525.